

# Spreading-rate dependence of melt extraction at mid-ocean ridges from mantle seismic refraction data

Daniel Lizarralde<sup>1</sup>, James B. Gaherty<sup>2</sup>, John A. Collins<sup>3</sup>, Greg Hirth<sup>3</sup> & Sangmyung D. Kim<sup>1</sup>

<sup>1</sup>School of Earth and Atmospheric Sciences, Georgia Institute of Technology, Atlanta, Georgia 30332, USA

<sup>2</sup>Lamont-Doherty Earth Observatory of Columbia University, Palisades, New York 10964, USA

<sup>3</sup>Department of Marine Geology and Geophysics, Woods Hole Oceanographic Institution, Woods Hole, Massachusetts 02543, USA

A variety of observations indicate that mid-ocean ridges produce less crust at spreading rates below 20 mm yr<sup>-1</sup> (refs 1–3), reflecting changes in fundamental ridge processes with decreasing spreading rate. The nature of these changes, however, remains uncertain, with end-member explanations being decreasing shallow melting<sup>3</sup> or incomplete melt extraction<sup>2</sup>, each due to the influence of a thicker thermal lid. Here we present results of a seismic refraction experiment designed to study mid-ocean ridge processes by imaging residual mantle structure. Our results reveal an abrupt lateral change in bulk mantle seismic properties associated with a change from slow to ultraslow palaeo-spreading rate. Changes in mantle velocity gradient, basement topography and crustal thickness all correlate with this spreading-rate change. These observations can be explained by variations in melt extraction at the ridge, with a gabbroic phase preferentially retained in the mantle at slower spreading rates. The estimated volume of retained melt balances the ~1.5-km difference in crustal thickness, suggesting that changes in spreading rate affect melt-extraction processes rather than total melting.

The processes of lithospheric formation at mid-ocean ridges (MORs)—mantle upwelling and corner flow, decompression melting, melt extraction, crustal accretion—are central to our understanding of mantle dynamics. The shallow upper mantle preserves structure inherited from and diagnostic of these processes, such as the patterns of melt depletion<sup>4</sup> and shear deformation<sup>5</sup>. These characteristics affect the mantle's seismic structure (for example, velocity and anisotropy). Imaging this structure can thus provide us with knowledge of the processes that have formed oceanic lithosphere at different times and under a variety of conditions.

The main FAIM (far-offset active-source imaging of the mantle) experiment transect, line 1, extends 800 km along a plate-kinematic flow line in the western mid-Atlantic, within a single spreading segment across lithosphere ranging in age from 108 to 157 million years (Myr) ago (ref. 6) (Fig. 1). Slow palaeo-spreading rates here enable us to investigate upper-mantle structure over a 35-Myr age span, and variations in palaeo-spreading rates during this time provide a means of evaluating the rate dependence of MOR processes. Eight pairs of vertical-component, 2-Hz ocean-bottom seismometers (OBSs) were deployed along line 1, spaced 80–120 km apart, and two OBSs were deployed at the ends of the orthogonal line 2, 150 km apart.

A primary result of the FAIM experiment is that mantle refractions sourced by airguns can be recorded at very far offsets (Fig. 2). On line 1, strong mantle refractions are observed to maximum offsets of 375 km by instruments on the eastern half of the transect. This phase is also observed to the maximum offset by both instruments on line 2. However, mantle refractions are not observed by instruments located on the western half of line 1. The lack of observed mantle refractions in the west most probably reflects a change in the propagation properties of the mantle, because noise

characteristics and instrument performance are the same in the east and west, and crustal phases are well recorded on all instruments. The transition from propagation to non-propagation of mantle refractions occurs near kilometre (km) 300 (eastward from the westernmost instrument), and it is abrupt, as evidenced by the coincident truncation at this location of refractions recorded by the instruments east of km 300 (Fig. 2). Primary mantle refractions from shots fired west of km 300 do not propagate back to the sea floor with recognizable energy. The simplest explanation for this energy dissipation is that the vertical velocity gradient west of km 300 is near zero or negative, consistent with conclusions from an explosive-source seismic study in the same region<sup>7</sup> (Fig. 1).

Mantle refraction travel times for lines 1 and 2 are well fitted with a mantle velocity structure that is approximately one-dimensional (Fig. 3). Velocity models for both lines require substantial vertical gradients (0.014 and 0.024 km s<sup>-1</sup> km<sup>-1</sup>), with the difference in average velocity indicating ~3% seismic anisotropy<sup>8</sup>. The velocity profile to 20-km depth is constrained by multiple instruments, but the deeper structure is constrained only by the far-offset Tecate travel times. These travel times are well fitted with a single linear gradient extending to a depth of 39 km, or by a model including a small velocity step near a depth of 30 km with a smaller gradient beneath. We prefer the velocity-step model because preliminary amplitude analysis indicates a weak preference for this model (Supplementary Fig. S7), and the deepest velocity in the single-gradient model is high (8.63 km s<sup>-1</sup>) relative to expectations for anisotropic, depleted peridotite at this depth<sup>9</sup>.

The steep positive velocity gradient in the east is not easily explained by MOR processes involving passive upwelling and efficient melt extraction. It is not explained by the predicted vertical variation in the extent of melting and associated depletion of a basaltic component. Seismic velocity increases with increasing depletion as mantle rock becomes more olivine- and magnesium-rich<sup>10</sup>, but the velocity change is small (<1%) and would produce a negative gradient in most models of decompression melting<sup>4</sup>. A

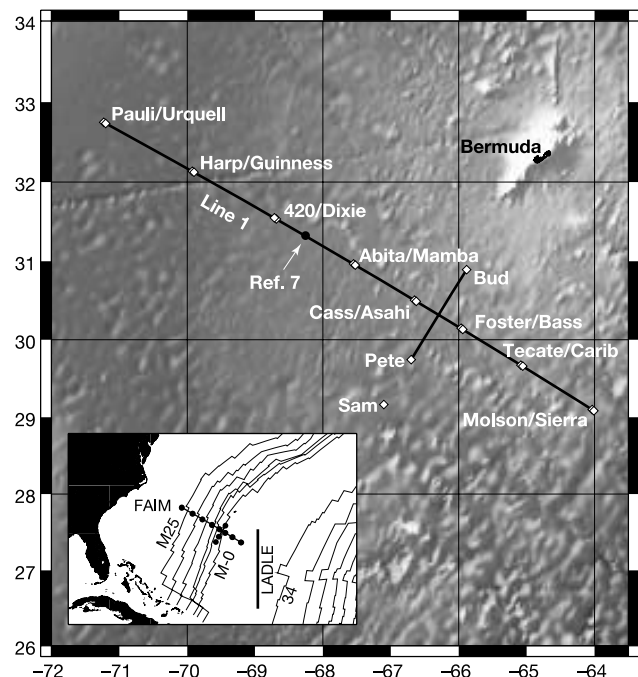


**Figure 1** FAIM experiment location and instrument layout. Line 1 lies along a plate-kinematic flow line. The experiment location of ref. 7 is indicated, and the LADLE<sup>19</sup> experiment location and lithospheric isochrons are indicated in the inset. LADLE, Lesser Antilles Deep Lithosphere Experiment.

vertical variation in anisotropy caused by the strain-induced crystal preferred orientation of olivine may yield a positive velocity gradient in one direction, but the gradient in the orthogonal direction should then be nearly flat, or even negative. The gradient is also not explained by the effects of increasing pressure and temperature with depth on elasticity. These effects are small and opposite in sign (Fig. 3), and they should be uniform throughout the region and thus unable to account for lateral transitions in vertical gradient. It is possible that the rougher basement east of km 425 (Fig. 4) indicates a more tectonic mode of extension here, with a more-fractured upper mantle. The closure of cracks with depth can produce important positive velocity gradients, but the predicted effect is too small and shallow to explain the observed gradients (Fig. 3). In the crust, the effect of tectonic cracks on seismic velocity is anisotropic, with a larger effect directed in the palaeo-spreading direction<sup>11,12</sup>. We would expect a similar anisotropic effect in the mantle, with a strong vertical gradient observed on line 1 and little or no gradient on line 2, but this pattern is not observed.

Our preferred explanation for the observed mantle velocity gradients is motivated by the rough correlation between the apparent velocity-gradient transition near km 300 and changes in basement morphology, crustal thickness and palaeo-spreading rate (Fig. 4). The half-spreading rate decreases from 14 to 13 mm yr<sup>-1</sup> at 140 Myr ago (km 325), to 8 mm yr<sup>-1</sup> at 132 Myr ago (km 425), and then increases to ~10 mm yr<sup>-1</sup> at ~125 Myr ago<sup>6</sup>. (The spreading rate after chron M-0 at km 550 is largely unconstrained. The value in Fig. 4 is an average rate for the entire Cretaceous quiet period, beginning 120 Myr ago.) The large decrease in spreading rate at

132 Myr ago is clearly correlated with roughening of basement topography, suggesting a shift to a more tectonic, less magmatic mode of extension. The crustal thickness measurements indicate that this slower-spreading crust is demonstrably thinner. Melt retained in the mantle at the spreading centre, now present as gabbroic inclusions, thus provides a possible explanation for the change to positive velocity gradients. In this scenario, melt extraction at very slow spreading rates becomes less efficient, owing to the increased effect of conductive cooling. Melt crystallized within the mantle, with the quantity of retained material increasing with decreasing depth, would systematically decrease velocities in proportion with the amount of retained melt. We evaluate this hypothesis with a simple mass-balance calculation. The crust east of km 425 is, on average, 1.4 km thinner than the crust west of km 300. The line-1 velocity gradient to a depth of 30 km can be explained by adding the equivalent of 1.5 km of gabbro (7 km s<sup>-1</sup>) to mantle rock with an intrinsic velocity of 8.5 km s<sup>-1</sup>. This simple calculation suggests that a melt-retention explanation for the change in velocity gradient along line 1 is plausible. This suggestion is supported by the fact that the observed gravity anomaly along line 1 is best explained by a lithosphere in isostatic equilibrium with the equivalent of ~1.5 km of crustal-density material distributed within the upper 20–40 km of the mantle (Supplementary Figs S1–S5). The spatial offset (~125 km) between the change in mantle velocity gradient and the change in spreading rate is consistent with the expected off-axis extent of the mantle–melt zone<sup>13</sup>, which also tends to support a melt-retention explanation (Supplementary Fig. S6).

A variety of observations suggest that the retention and crystallization of melt in the mantle is common in slow-spreading environments. The composition of basalts emplaced at slow-spreading ridges suggests that fractional crystallization occurs within the upper mantle to depths of 18 km below the sea floor<sup>14</sup>. The composition of dredged plagioclase peridotites<sup>15</sup> is consistent with this notion. Recent drilling along the mid-Atlantic ridge on Ocean Drilling Program Leg 209 recovered gabbroic rocks, found as intrusions and impregnations in residual peridotite, which crystal-

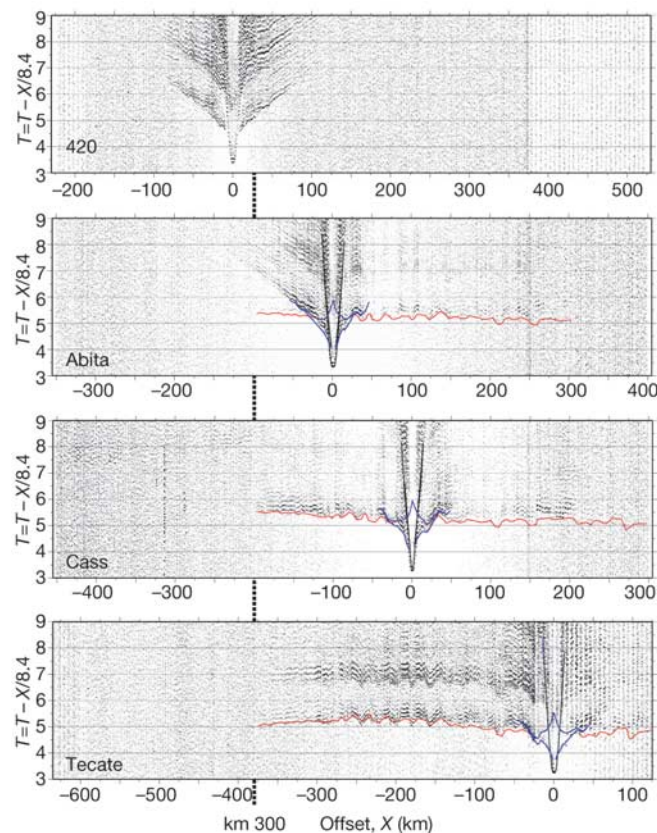


**Figure 2** Profiles from FAIM line 1 plotted at reduced travel time  $T$  (in seconds), using a reduction velocity  $V$  of 8.4 km s<sup>-1</sup>. Predicted travel times are overlain (black, sea floor and sediments; blue, crustal refractions; red, mantle refractions). The mantle-refraction phase terminates at a distinct location near model km 300. Mantle refractions do not propagate from west of km 300, as seen on instrument 420.

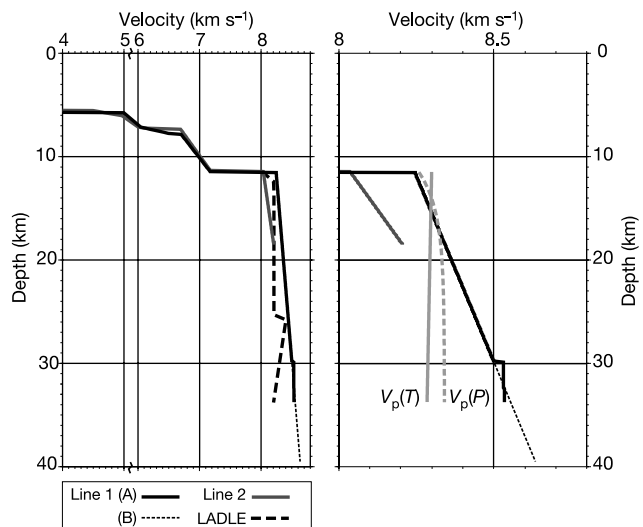


**Figure 3** Velocity depth profiles at the line 1/line 2 crossing based on isotropic ray tracing of FAIM travel times. The two line 1 models, A and B, fit the travel-time data equally well, but amplitude analysis favours model B somewhat. The velocity profile based on the LADLE<sup>19</sup> transect, at an azimuth of ~0° (~60° off the flow line), lies between the line 1 and line 2 results. Predicted pressure dependence (based on laboratory measurements on dunite<sup>28</sup> and a model of the pressure dependence of P-wave velocity,  $V_p(P)$ , which isolates the effects of microcracks<sup>10</sup>) and temperature<sup>30</sup> dependence,  $V_p(T)$ , are also indicated; the combined effects nearly cancel but predict a slightly negative gradient below ~22 km depth.

lized at depths of up to 17 km beneath the sea floor and are believed to comprise 20–40% of the upper mantle at this location<sup>16</sup>.

Our interpretation of the FAIM results suggests that, for slow-spreading systems, spreading rate has a greater effect on melt extraction than on total melt production. This conclusion differs from an interpretation of data from the ultraslow-spreading (half-rate 3–6.5 mm yr<sup>-1</sup>) Gakkel Ridge, where anomalously thin crust (1.9–3.3 km thick) was taken as evidence for reduced melt production<sup>17</sup>. The Gakkel experiment placed some constraints on the uppermost mantle structure, where slow velocities ( $V_p \approx 7.5$ – $7.8$  km s<sup>-1</sup>) just below the Moho were interpreted as serpentinized peridotite. An alternative interpretation is that the slow upper-mantle velocities beneath Gakkel are due in part to gabbroic inclusions present in greater proportion to balance the thin crust. Similarly, the systematically enriched rare-earth-element (REE) concentrations observed in basalts from very-slow-spreading ridges have been interpreted to indicate deeper melting with nearly complete melt extraction at these ridges<sup>3</sup>. Numerical models suggest that this REE enrichment might also be expected in a passively driven system where the off-axis portion of the distributed melt network remains largely trapped, and the crust-forming melts are predominantly extracted from the mantle upwelling directly beneath the ridge axis<sup>13</sup>, the hottest portion of the system (Supplementary Fig. S6).

The presence of a mantle gabbroic component may also provide an explanation for a possible discontinuity near a depth of 30 km, which is similar (~35 km) to the depth where the transformation of olivine tholeiite to eclogite begins, at ~1 GPa (ref. 18). The requirement of this velocity discontinuity is tentative, and further analyses are needed to constrain its existence better. Nevertheless, similar discontinuities have been inferred from other very large offset refraction experiments<sup>19–22</sup>, with a gabbro-to-eclogite transformation suggested as an explanation. If this explanation is correct, then the apparent common occurrence of such a boundary suggests

that significant quantities of melt may routinely be retained in the mantle under a variety of conditions. □

Methods

Experiment design

Detailed seismic imaging of the uppermost oceanic mantle, to depths comparable to the onset of melting at 60–90 km, can be achieved with active-source techniques employing very large source-to-receiver offsets. A small number of such studies have been carried out in the oceans using explosive sources<sup>19–22</sup>. These experiments identified large velocity gradients and velocity discontinuities in the upper 50 km of the mantle interpreted as compositional layering. Other than these studies, detailed knowledge of upper-mantle seismic structure away from a ridge is surprisingly poor. This is due in large part to the cost and inherent safety risks of explosive sources. Our experiment was designed to acquire large-offset marine refraction data using airguns rather than explosives. Mantle phases from airgun sources are commonly recorded at 200–300 km offsets by land-based seismometers<sup>23,24</sup>. Similar observations in the oceans had not been made before the FAIM experiment, however, largely owing to the presence of water-borne ‘previous shot’ noise (PSN)<sup>25</sup> endemic at large offsets during airgun shooting with typical shot intervals of 90 s or less. The relationship between shot interval,  $\Delta t$ , and the offset,  $X_{PSN}$ , at which a mantle refraction from a particular shot and water-borne energy from the previous shot arrive simultaneously is  $\Delta t = X_{PSN}(1/V_W - 1/V_M)$ , where  $V_W$  and  $V_M$  are the water and mantle propagation velocities. To record mantle phases at 600-km offset, for example, without the interference of high-energy PSN, a shot interval of ~6 min is required. The two principal elements of the shooting strategy were thus long shot intervals and repetition of shots in the same (or nearly the same) location to enable signal-to-noise enhancement through stacking. The source for the experiment was a ~150-litre, 20-element airgun array. Two modes of shooting were tested, ‘circle’ shots and ‘on-distance’ shooting. The circle-shooting mode was tested on the eastern 150 km and western 36 km of line 1. Circle shooting involved shooting at a prescribed shot interval while steaming in a circle with radius 1 km, the tightest possible with the towed source array. This is a time-efficient means of generating many shots near a single location. Between 17 and 36 shots were fired along each circle. Static corrections were applied to the traces from each circle, and the traces were stacked. We found that substantial basement roughness and the azimuthal dependence of the source-array signature rendered this mode of shooting problematic. On-distance shooting, where the source is triggered at predefined points by the navigation system, is the simplest and most effective of these two modes; it was used during most of the experiment. A source-point separation of 1 km was used, giving a shot interval of ~6 min. On line 1, these source-points were revisited on multiple transits of portions of the line, with one to seven shots fired at each point. Stacking of these co-located shots clearly improves the signal-to-noise ratio of the data, but we found that profiles consisting of unstacked single shots are of sufficient quality to enable accurate identification and picking of refraction travel times, even at the largest offsets. This result suggests that a very simple shooting strategy may suffice for other experiments of this type.

Velocity modelling

Mantle velocities were determined for line 1 (east of km 300) and line 2 by two-dimensional, ray-trace modelling<sup>26</sup> of first-arrival travel times. Sediment thickness and basement topography were constrained using multi-channel seismic data from the IPOD/USGS transect<sup>27</sup>, which is coincident with the FAIM transect. Crustal thickness and velocity were constrained at the instrument locations using observed crustal phases (Fig. 3). These constraints were used to form the two-dimensional ray-tracing model within which the mantle velocity structure is nearly one-dimensional. The requirement of substantial vertical mantle velocity gradients is indicated by the continuously increasing apparent velocity with offset observed on the Tecate profile, for example, on which the largest-offset first arrivals are observed (Fig. 2).

Received 24 June; accepted 29 October 2004; doi:10.1038/nature03140.

- Chen, Y. J. Oceanic crustal thickness versus spreading rate. *Geophys. Res. Lett.* **19**, 753–756 (1992).
- Cannat, M. How thick is the magmatic crust at slow spreading oceanic ridges? *J. Geophys. Res.* **101**, 2847–2857 (1996).
- White, R. S., Minshull, T. A., Bickle, M. J. & Robinson, C. J. Melt generation at very slow-spreading oceanic ridges: Constraints from geochemical and geophysical data. *J. Petrol.* **42**, 1171–1196 (2001).
- Langmuir, C. H., Klein, E. M. & Plank, T. in *Mantle Flow and Melt Generation at Mid-Ocean Ridges* (eds Morgan, J. P., Blackman, D. K. & Sinton, J. M.) 183–281 (Geophysical Monograph 71, American Geophysical Union, Washington DC, 1993).
- Blackman, D. K. & Kendall, J.-M. Seismic anisotropy in the upper mantle. 2. Predictions for current plate boundary flow models. *Geochem. Geophys. Geosyst.* **3**, doi:10.1029/2001GC000247 (2002).
- Müller, R. D., Walter, W. R., Royer, J.-Y., Gahagan, L. M. & Sclater, J. G. Digital isochrones of the world’s ocean floor. *J. Geophys. Res.* **102**, 3211–3214 (1997).
- Purdy, G. M. The seismic structure of 140 Myr old crust in the western central Atlantic Ocean. *Geophys. J. R. Astron. Soc.* **72**, 115–137 (1983).
- Gaherty, J. B., Lizarralde, D., Collins, J. A., Hirth, G. & Kim, S. D. Mantle deformation during slow seafloor spreading constrained by observations of seismic anisotropy in the western Atlantic. *Earth Planet. Sci. Lett.* (in the press).
- Ben Ismail, W. & Mainprice, D. An olivine fabric database: an overview of upper mantle fabrics and seismic anisotropy. *Tectonophysics* **296**, 145–157 (1998).
- Jordan, T. H. in *The Mantle Sample: Inclusions in Kimberlites and Other Volcanics* (eds Boyd, F. R. & Meyer, H. O. A.) 1–14 (American Geophysical Union, Washington DC, 1979).
- Stephen, R. A. Seismic anisotropy in the upper oceanic crust. *J. Geophys. Res.* **90**, 11383–11396 (1985).
- Detrick, R. S., Toomey, D. R. & Collins, J. A. Three-dimensional upper crustal heterogeneity and anisotropy around Hole 504B from seismic tomography. *J. Geophys. Res.* **103**, 30485–30504 (1998).
- Spiegelman, M. & Reynolds, J. R. Combined dynamic and geochemical evidence for convergent melt

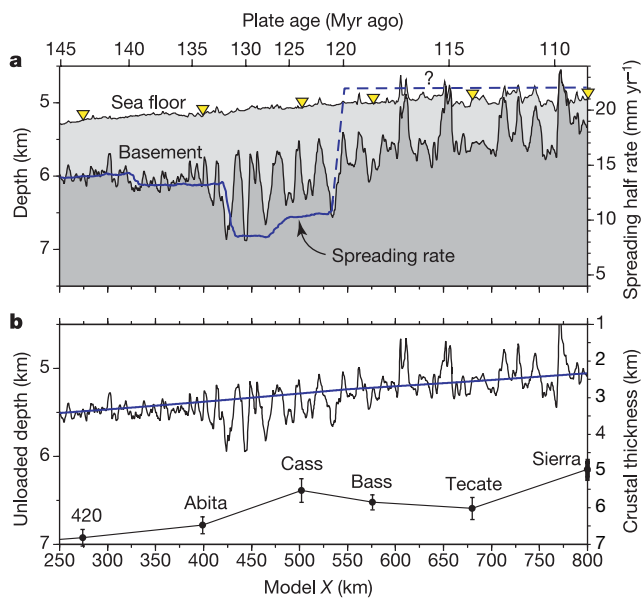


**Figure 4** Basement depth, spreading rate and crustal thickness. **a**, FAIM line 1 sea floor and basement depths from multi-beam and multi-channel seismic constraints, and spreading rate<sup>9</sup>. The increase indicated at 120 Myr is a jump to the average value for the Cretaceous quiet zone. Note strong correlation between basement morphology and spreading rate. Yellow triangles indicate instrument locations. **b**, Sediment unloaded basement depth, depth predicted from plate cooling (blue line), and crustal thickness estimates for the indicated stations.

flow beneath the East Pacific Rise. *Nature* **402**, 282–285 (1999).

14. Grove, T. L., Kinzler, R. J. & Bryan, W. B. in *Mantle Flow and Melt Generation at Mid-Ocean Ridges* (eds Morgan, J. P., Blackman, D. K. & Sinton, J. M.) 281–310 (Geophysical Monograph 71, American Geophysical Union, Washington DC, 1993).
15. Dick, H. J. B. in *Magnetism in the Ocean Basins* (eds Saunders, A. D. & Norry, M. J.) 71–105 (Geol. Soc. Spec. Publ. No. 42, Bath, 1989).
16. Kelemen, P. B., Kikawa, E., Miller, D. J. & The Leg 209 Scientific Party. ODP Leg 209 drills into mantle peridotite along the mid-Atlantic ridge from 14°N to 16°N. *JOIDES J.* **30**, 14–19 (2004).
17. Jokat, W. *et al.* Geophysical evidence for reduced melt production on the Arctic ultraslow Gakkel mid-ocean ridge. *Nature* **423**, 962–965 (2003).
18. Green, D. H. & Ringwood, A. E. An experimental investigation of gabbro to eclogite transformation and its petrological applications. *Geochim. Cosmochim. Acta* **31**, 767–833 (1967).
19. LADLE Study Group. A lithospheric seismic refraction profile in the western North Atlantic Ocean. *Geophys. J. R. Astron. Soc.* **75**, 23–69 (1983).
20. Asada, T. & Shimimura, H. Long-range refraction experiments in deep ocean. *Tectonophysics* **56**, 67–82 (1979).
21. Zverev, S. M. & Yaroshevskiy, G. A. in *Composition, Structure, and Dynamics of Lithosphere-Asthenosphere System* (eds Fuchs, K. & Froidevaux, C.) 273–290 (Geodyn. Ser. 16, American Geophysical Union, 1987).
22. Goodman, D. & Bibee, L. D. Measurements and modelling of possible mantle constituents from a long-line seismic refraction experiment in the West Philippine Basin. *Geophys. J. Int.* **106**, 667–675 (1991).
23. Chian, D., Hall, J. & Marillier, F. Lithospheric wide-angle seismic profiles using stacked airgun shots. *Geophys. Res. Lett.* **23**, 2077–2080 (1996).
24. Lizarralde, D. & Holbrook, W. S. US mid-Atlantic margin structure and early thermal evolution. *J. Geophys. Res.* **102**, 22855–22875 (1997).
25. Nakamura, Y., Donoho, P. L., Roper, P. H. & McPherson, P. M. Large-offset seismic surveying using ocean-bottom seismographs and air guns: Instrumentation and field technique. *Geophysics* **52**, 1601–1611 (1987).
26. Zelt, C. A. & Smith, R. B. Seismic traveltime inversion for 2-D crustal velocity structure. *Geophys. J. Int.* **108**, 16–34 (1992).
27. Grow, J. A. & Markl, R. G. IPOD-USGS multichannel seismic reflection profile from Cape Hatteras to the Mid-Atlantic ridge. *Geology* **5**, 625–630 (1977).
28. Christensen, N. I. Compressional wave velocities in possible mantle rocks to pressures of 30 kilobars. *J. Geophys. Res.* **79**, 407–412 (1974).
29. Greenfield, R. J. & Graham, E. K. Application of a simple relation for describing wave velocity as a function of pressure in rocks containing microcracks. *J. Geophys. Res.* **101**, 5643–5652 (1996).
30. Goes, S. & Govers, R. Shallow mantle temperatures under Europe from P and S wave tomography. *J. Geophys. Res.* **105**, 11153–11169 (2000).

**Supplementary Information** accompanies the paper on [www.nature.com/nature](http://www.nature.com/nature).

**Acknowledgements** We thank the Lamont Marine Office and the captain and crew of the RV *Maurice Ewing* for their efforts during cruise EW-0106. The efforts of J. DiBernardo, J. Stennet and J. Diebold are appreciated. This work was supported by the US National Science Foundation.

**Competing interests statement** The authors declare that they have no competing financial interests.

**Correspondence** and requests for materials should be addressed to D.L. ([danl@eas.gatech.edu](mailto:danl@eas.gatech.edu)).

## Spatial scaling of microbial eukaryote diversity

Jessica L. Green<sup>1\*</sup>, Andrew J. Holmes<sup>2</sup>, Mark Westoby<sup>1</sup>, Ian Oliver<sup>3</sup>, David Briscoe<sup>1</sup>, Mark Dangerfield<sup>1</sup>, Michael Gillings<sup>1</sup> & Andrew J. Beattie<sup>1</sup>

<sup>1</sup>Key Centre for Biodiversity and Bioresources, Department of Biological Sciences, Macquarie University, New South Wales 2109, Australia

<sup>2</sup>School of Molecular and Microbial Biosciences, The University of Sydney, New South Wales 2006, Australia

<sup>3</sup>New South Wales Department of Infrastructure, Planning and Natural Resources, P.O. Box U245, University of New England, Armidale, New South Wales 2351, Australia

\* Present address: School of Natural Sciences, University of California, Merced, P.O. Box 2039, Merced, California 95344, USA

Patterns in the spatial distribution of organisms provide important information about mechanisms that regulate the diversity of life and the complexity of ecosystems<sup>1,2</sup>. Although microorganisms may comprise much of the Earth's biodiversity<sup>3,4</sup> and have critical roles in biogeochemistry and ecosystem functioning<sup>5–7</sup>, little is known about their spatial diversification. Here we

present quantitative estimates of microbial community turnover at local and regional scales using the largest spatially explicit microbial diversity data set available (>10<sup>6</sup> sample pairs). Turnover rates were small across large geographical distances, of similar magnitude when measured within distinct habitats, and did not increase going from one vegetation type to another. The taxa–area relationship of these terrestrial microbial eukaryotes was relatively flat (slope  $z = 0.074$ ) and consistent with those reported in aquatic habitats<sup>8,9</sup>. This suggests that despite high local diversity, microorganisms may have only moderate regional diversity. We show how turnover patterns can be used to project taxa–area relationships up to whole continents. Taxa dissimilarities across continents and between them would strengthen these projections. Such data do not yet exist, but would be feasible to collect.

Ecologists studying macroorganisms have long recognized that beta-diversity (how community composition changes across a landscape) is central to understanding the forces responsible for the magnitude and variability of biodiversity. Patterns of beta-diversity can offer valuable clues to the relative influence of dispersal limitation, environmental heterogeneity, and environmental and evolutionary change in shaping the structure of ecological communities<sup>10–14</sup>. Despite an increasing awareness that spatial patterning of soil microbiota can have important aboveground consequences in regard to plant community structure and ecosystem functioning<sup>5,6,15,16</sup>, microbial beta-diversity patterns are largely unknown. Inadequate sampling has been a major limitation and scientists are only now beginning to explore emergent patterns and principles that may be common to microbes, plants and animals<sup>17,18</sup>. Thus, whereas it is widely accepted that the similarity in plant and animal community composition decays with increasing distance between samples<sup>11,13,19</sup>, patterns of microbial turnover in terrestrial environments remain unstudied. Here, we test whether similarity in microbial eukaryote community composition decays with geographical distance as observed in macroorganisms. We also explore how these biodiversity turnover patterns are influenced by strong habitat-related environmental discontinuities. Finally, we apply spatial scaling theory to these turnover patterns to predict how microbial biodiversity might increase with sampling area from local to continental scales in Australia.

A total of 1,536 soil samples were collected in arid Australia using a spatially explicit nested design. The design resulted in 1,117,880 pairwise sample comparisons, with distances ranging from 1 m to ~100 km represented by multiple replicate sample pairs. Samples were taken from four distinct land systems that varied substantially in geology, topography and native vegetation (see Supplementary Information). We measured the similarity between any two samples using the Sørensen index, defined as the number of taxa in common divided by the average number of taxa in the two samples<sup>20</sup>. The rate at which Sørensen similarity decays with increasing distance between samples (the distance–decay relationship) can be directly related to the species–area relationship<sup>21</sup>. Other measures of similarity based on presence/absence of data yielded qualitatively similar results to those reported here.

We characterized the beta-diversity of ascomycete fungi by automated ribosomal RNA intergenic spacer analysis (ARISA), a commonly used DNA-based community fingerprinting method<sup>22–24</sup>. ARISA is a high-resolution, highly reproducible technique for detecting differences between complex fungal communities<sup>22</sup>. We chose ARISA over DNA sequencing because it allowed assessment of microbial community turnover at an unparalleled sample size and spatial scale. ARISA exploits variability in the length of the intervening transcribed spacer regions of rRNA genes (ITS) to sort samples rapidly into operational taxonomic units (OTUs). Members of different species may share the same ITS fragment size<sup>22</sup>. Although ARISA assays a different taxonomic resolution than species, it is a consistent measure of community composition